

# A generalized energy-based modeling framework with application to field/circuit coupled problems

Robert Altmann<sup>a</sup>, Idoia Cortes Garcia<sup>b</sup>, Elias Paakkunainen<sup>c,d,\*</sup>,  
Philipp Schulze<sup>e</sup>, Sebastian Schöps<sup>c</sup>

<sup>a</sup>*Institute of Analysis and Numerics, Otto von Guericke University  
Magdeburg, Magdeburg, 39106, Germany*

<sup>b</sup>*Department of Mechanical Engineering, Eindhoven University of  
Technology, Eindhoven, 5600 MB, The Netherlands*

<sup>c</sup>*Institute for Accelerator Science and Electromagnetic Fields, Technical University of  
Darmstadt, Darmstadt, 64289, Germany*

<sup>d</sup>*Electrical Engineering Unit, Tampere University, Tampere, 33720, Finland*

<sup>e</sup>*Institute of Mathematics, Technische Universität Berlin, Berlin, 10623, Germany*

---

## Abstract

This paper presents a generalized energy-based modeling framework extending recent formulations tailored for differential–algebraic equations. The proposed structure, inspired by the port-Hamiltonian formalism, ensures passivity, preserves the power balance, and facilitates the consistent interconnection of subsystems. A particular focus is put on low-frequency power applications in electrical engineering. Stranded, solid, and foil conductor models are investigated in the context of the eddy current problem. Each conductor model is shown to fit into the generalized energy-based structure, which allows their structure-preserving coupling with electrical circuits described by modified nodal analysis. Theoretical developments are validated through a numerical simulation of an oscillator circuit, demonstrating energy conservation in lossless scenarios and controlled dissipation when eddy currents are present.

*Keywords:* energy-based modeling, field/circuit problems, differential–algebraic equations

---

\*Corresponding author: Elias Paakkunainen (e-mail: [elias.paakkunainen@tu-darmstadt.de](mailto:elias.paakkunainen@tu-darmstadt.de)).

## 1. Introduction

In recent years, energy-based modeling via port-Hamiltonian (pH) formulations has received more and more attention; cf. [1, 2] for a general overview. The pH framework generalizes classical Hamiltonian systems by allowing for energy dissipation as well as energy exchange with the environment. Moreover, the corresponding structure implies a power balance and ensures passivity, i.e., the system may not internally generate energy. Often, the power balance also implies (Lyapunov) stability, e.g., if the Hamiltonian is a squared norm of the state. Furthermore, power-preserving interconnections of pH systems result in an overall system which is again pH. This makes the framework especially suitable for network modeling and control [3, 4, 5, 6]. PH structures have been identified in various application areas, including chemistry [7, 8, 9], electrical engineering [10, 11, 12, 13, 14], and mechanics [15, 16, 17, 18]. Structure-preserving discretization and model order reduction techniques are presented, e.g., in [19, 20, 21, 22, 23, 24].

Recently, a new representation of energy-based models has been introduced in [25] that appears to be especially suitable for differential–algebraic equation systems (DAE). Similarly to classical pH formulations, it implies a power balance, is preserved under power-preserving interconnections, and allows for structure-preserving discretization and model reduction. Moreover, in some applications, it allows to obtain energy-based formulations with fewer state variables compared to the pH-DAE formulations presented in [26, 27]. In addition, the new framework also includes systems of index 3, whereas the linear pH-DAE formulation in [26] is restricted to systems with an index of at most 2, cf. [28].

This paper introduces a generalization of the original energy-based framework to account for practically relevant models from electrical engineering, i.e., modified nodal analysis (MNA) for the description of electric circuits including lumped elements and refined models describing three-dimensionally resolved electromagnetic fields based on (quasistatic) Maxwell’s equations. Such coupled systems arise in various practical situations, e.g., when simulating electric machines or accelerator circuits; see [29, 30]. Mathematically, the field-circuit coupling is established by prolongation and restriction operators which can be related to conductor models, e.g., stranded, solid, or foil models [31, 32, 33, 34]. All models, i.e., circuit and field, are known to be DAEs of index up to two depending on the circuit topology; see [35, 36, 37].

## 2. Energy-Based Modeling

In [25], the authors have introduced a structured energy-based formulation which is especially suitable for DAEs. In this paper, we propose a generalization that allows for additional algebraic components in the variables, as this is important for the MNA model to be investigated later. The new formulation reads

$$\begin{bmatrix} \nabla_{\mathbf{z}_1} \mathcal{H}(\mathbf{z}_1, \mathbf{z}_2) \\ \mathcal{E} \frac{d}{dt} \mathbf{z}_2 \\ 0 \end{bmatrix} = (\mathcal{J} - \mathcal{R}) \begin{bmatrix} \frac{d}{dt} \mathbf{z}_1 \\ \mathbf{e}(\mathbf{z}_1, \mathbf{z}_2) \\ \mathbf{z}_3 \end{bmatrix} + \mathcal{B} \mathbf{u} \quad (1)$$

with state  $\mathbf{z} = (\mathbf{z}_1, \mathbf{z}_2, \mathbf{z}_3): [t_0, t_f] \rightarrow \mathbb{R}^{n_1} \times \mathbb{R}^{n_2} \times \mathbb{R}^{n_3}$ , input  $\mathbf{u}: [t_0, t_f] \rightarrow \mathbb{R}^m$ , Hamiltonian  $\mathcal{H}: \mathbb{R}^{n_1} \times \mathbb{R}^{n_2} \rightarrow \mathbb{R}$ , effort  $\mathbf{e}: \mathbb{R}^{n_1} \times \mathbb{R}^{n_2} \rightarrow \mathbb{R}^{n_2}$ , and coefficient matrices  $\mathcal{E} \in \mathbb{R}^{n_2 \times n_2}$ ,  $\mathcal{J}, \mathcal{R} \in \mathbb{R}^{n \times n}$ ,  $\mathcal{B} \in \mathbb{R}^{n \times m}$  with  $n := n_1 + n_2 + n_3$ . In particular,  $\mathcal{J}$  must be skew-symmetric and  $\mathcal{R}$  symmetric and positive semi-definite. Moreover, we assume that

$$\mathcal{E}^\top \mathbf{e}(\mathbf{z}_1, \mathbf{z}_2) = \nabla_{\mathbf{z}_2} \mathcal{H}(\mathbf{z}_1, \mathbf{z}_2),$$

which is inspired by the port-Hamiltonian structure introduced in [27]. In addition, we have an equation for the output  $\mathbf{y}: [t_0, t_f] \rightarrow \mathbb{R}^m$ , given by

$$\mathbf{y} = \mathcal{B}^\top \begin{bmatrix} \frac{d}{dt} \mathbf{z}_1 \\ \mathbf{e}(\mathbf{z}_1, \mathbf{z}_2) \\ \mathbf{z}_3 \end{bmatrix}. \quad (2)$$

**Remark 1.** *The matrix  $\mathcal{E}$  is not necessarily invertible. However, if  $\mathcal{E}$  equals the identity, then  $\mathbf{e}(\mathbf{z}_1, \mathbf{z}_2) = \nabla_{\mathbf{z}_2} \mathcal{H}(\mathbf{z}_1, \mathbf{z}_2)$  and we regain the basic model from [25], namely*

$$\begin{bmatrix} \nabla_{\mathbf{z}_1} \mathcal{H}(\mathbf{z}_1, \mathbf{z}_2) \\ \frac{d}{dt} \mathbf{z}_2 \\ 0 \end{bmatrix} = (\mathcal{J} - \mathcal{R}) \begin{bmatrix} \frac{d}{dt} \mathbf{z}_1 \\ \nabla_{\mathbf{z}_2} \mathcal{H}(\mathbf{z}_1, \mathbf{z}_2) \\ \mathbf{z}_3 \end{bmatrix} + \mathcal{B} \mathbf{u}. \quad (3)$$

### 2.1. Power Balance and Interconnections

We first prove that systems of the form (1)–(2) follow the typical power balance.

**Lemma 2** (Energy dissipation). *The energy satisfies  $\frac{d}{dt} \mathcal{H} \leq \langle \mathbf{y}, \mathbf{u} \rangle$ . In particular, system (1)–(2) is energy dissipative for  $\mathbf{u} = 0$ .*

*Proof.* A direct calculation shows

$$\begin{aligned}
\frac{d}{dt}\mathcal{H} &= \langle \nabla_{\mathbf{z}_1}\mathcal{H}(\mathbf{z}_1, \mathbf{z}_2), \frac{d}{dt}\mathbf{z}_1 \rangle + \langle \mathbf{e}(\mathbf{z}_1, \mathbf{z}_2), \mathcal{E}\frac{d}{dt}\mathbf{z}_2 \rangle \\
&= \left\langle \begin{bmatrix} \frac{d}{dt}\mathbf{z}_1 \\ \mathbf{e}(\mathbf{z}_1, \mathbf{z}_2) \\ \mathbf{z}_3 \end{bmatrix}, \begin{bmatrix} \nabla_{\mathbf{z}_1}\mathcal{H}(\mathbf{z}_1, \mathbf{z}_2) \\ \mathcal{E}\frac{d}{dt}\mathbf{z}_2 \\ 0 \end{bmatrix} \right\rangle \\
&= -\left\langle \begin{bmatrix} \frac{d}{dt}\mathbf{z}_1 \\ \mathbf{e}(\mathbf{z}_1, \mathbf{z}_2) \\ \mathbf{z}_3 \end{bmatrix}, \mathcal{R} \begin{bmatrix} \frac{d}{dt}\mathbf{z}_1 \\ \mathbf{e}(\mathbf{z}_1, \mathbf{z}_2) \\ \mathbf{z}_3 \end{bmatrix} \right\rangle + \left\langle \begin{bmatrix} \frac{d}{dt}\mathbf{z}_1 \\ \mathbf{e}(\mathbf{z}_1, \mathbf{z}_2) \\ \mathbf{z}_3 \end{bmatrix}, \mathcal{B}\mathbf{u} \right\rangle \leq \langle \mathbf{y}, \mathbf{u} \rangle.
\end{aligned}$$

The special case  $\mathbf{u} = 0$  clearly yields  $\frac{d}{dt}\mathcal{H} \leq 0$ .  $\square$

A second important property is that systems of the form (1)–(2) can be coupled, leading again to a system of the same structure.

**Lemma 3** (Structure-preserving interconnection). *Consider two systems of the form (1)–(2), namely*

$$\begin{aligned}
\begin{bmatrix} \partial_1\mathcal{H}^{[i]} \\ \mathcal{E}^{[i]}\frac{d}{dt}\mathbf{z}_2^{[i]} \\ 0 \end{bmatrix} &= (\mathcal{J}^{[i]} - \mathcal{R}^{[i]}) \begin{bmatrix} \frac{d}{dt}\mathbf{z}_1^{[i]} \\ \mathbf{e}^{[i]}(\mathbf{z}_1^{[i]}, \mathbf{z}_2^{[i]}) \\ \mathbf{z}_3^{[i]} \end{bmatrix} + \mathcal{B}^{[i]}\mathbf{u}^{[i]}, \\
\mathbf{y}^{[i]} &= \mathcal{B}^{[i]\top} \begin{bmatrix} \frac{d}{dt}\mathbf{z}_1^{[i]} \\ \mathbf{e}^{[i]}(\mathbf{z}_1^{[i]}, \mathbf{z}_2^{[i]}) \\ \mathbf{z}_3^{[i]} \end{bmatrix}
\end{aligned}$$

with respective states  $\mathbf{z}^{[1]}$ ,  $\mathbf{z}^{[2]}$ , energy functions  $\mathcal{H}^{[1]}$ ,  $\mathcal{H}^{[2]}$ , efforts  $\mathbf{e}^{[1]}$ ,  $\mathbf{e}^{[2]}$ , and the short notation  $\partial_k\mathcal{H}^{[i]} = \nabla_{\mathbf{z}_k^{[i]}}\mathcal{H}^{[i]}(\mathbf{z}_1^{[i]}, \mathbf{z}_2^{[i]})$ . Then an interconnection of the form

$$\begin{bmatrix} \mathbf{u}^{[1]} \\ \mathbf{u}^{[2]} \end{bmatrix} = (\mathcal{F}_{skew} - \mathcal{F}_{sym}) \begin{bmatrix} \mathbf{y}^{[1]} \\ \mathbf{y}^{[2]} \end{bmatrix} + \begin{bmatrix} \tilde{\mathbf{u}}^{[1]} \\ \tilde{\mathbf{u}}^{[2]} \end{bmatrix}$$

with  $\mathcal{F}_{skew} = -\mathcal{F}_{skew}^\top$  and positive semi-definite  $\mathcal{F}_{sym} = \mathcal{F}_{sym}^\top$  yields again a system of the form (1)–(2).

*Proof.* We define the new states

$$\mathbf{z}_1 := \begin{bmatrix} \mathbf{z}_1^{[1]} \\ \mathbf{z}_1^{[2]} \\ \mathbf{z}_1^{[1]} \end{bmatrix}, \quad \mathbf{z}_2 := \begin{bmatrix} \mathbf{z}_2^{[1]} \\ \mathbf{z}_2^{[2]} \\ \mathbf{z}_2^{[2]} \end{bmatrix}, \quad \mathbf{z}_3 := \begin{bmatrix} \mathbf{z}_3^{[1]} \\ \mathbf{z}_3^{[2]} \\ \mathbf{z}_3^{[2]} \end{bmatrix}$$

as well as the in- and outputs

$$\mathbf{u} := \begin{bmatrix} \mathbf{u}^{[1]} \\ \mathbf{u}^{[2]} \end{bmatrix}, \quad \tilde{\mathbf{u}} := \begin{bmatrix} \tilde{\mathbf{u}}^{[1]} \\ \tilde{\mathbf{u}}^{[2]} \end{bmatrix}, \quad \mathbf{y} := \begin{bmatrix} \mathbf{y}^{[1]} \\ \mathbf{y}^{[2]} \end{bmatrix}.$$

We consider  $\mathcal{H}(\mathbf{z}_1, \mathbf{z}_2) := \mathcal{H}^{[1]}(\mathbf{z}_1^{[1]}, \mathbf{z}_2^{[1]}) + \mathcal{H}^{[2]}(\mathbf{z}_1^{[2]}, \mathbf{z}_2^{[2]})$  as the Hamiltonian of the coupled system. Assuming the block structure

$$\mathcal{J}^{[i]} = \begin{bmatrix} \mathcal{J}_{11}^{[i]} & \mathcal{J}_{12}^{[i]} & \mathcal{J}_{13}^{[i]} \\ -\mathcal{J}_{12}^{[i]\top} & \mathcal{J}_{22}^{[i]} & \mathcal{J}_{23}^{[i]} \\ -\mathcal{J}_{13}^{[i]\top} & -\mathcal{J}_{23}^{[i]\top} & \mathcal{J}_{33}^{[i]} \end{bmatrix}, \quad \mathcal{R}^{[i]} = \begin{bmatrix} \mathcal{R}_{11}^{[i]} & \mathcal{R}_{12}^{[i]} & \mathcal{R}_{13}^{[i]} \\ \mathcal{R}_{12}^{[i]\top} & \mathcal{R}_{22}^{[i]} & \mathcal{R}_{23}^{[i]} \\ \mathcal{R}_{13}^{[i]\top} & \mathcal{R}_{23}^{[i]\top} & \mathcal{R}_{33}^{[i]} \end{bmatrix}, \quad \mathcal{B}^{[i]} = \begin{bmatrix} \mathcal{B}_1^{[i]} \\ \mathcal{B}_2^{[i]} \\ \mathcal{B}_3^{[i]} \end{bmatrix},$$

we define the matrices

$$\mathcal{J} := \begin{bmatrix} \mathcal{J}_{11}^{[1]} & 0 & \mathcal{J}_{12}^{[1]} & 0 & \mathcal{J}_{13}^{[1]} & 0 \\ 0 & \mathcal{J}_{11}^{[2]} & 0 & \mathcal{J}_{12}^{[2]} & 0 & \mathcal{J}_{13}^{[2]} \\ -\mathcal{J}_{12}^{[1]\top} & 0 & \mathcal{J}_{22}^{[1]} & 0 & \mathcal{J}_{23}^{[1]} & 0 \\ 0 & -\mathcal{J}_{12}^{[2]\top} & 0 & \mathcal{J}_{22}^{[2]} & 0 & \mathcal{J}_{23}^{[2]} \\ -\mathcal{J}_{13}^{[1]\top} & 0 & -\mathcal{J}_{23}^{[1]\top} & 0 & \mathcal{J}_{33}^{[1]} & 0 \\ 0 & -\mathcal{J}_{13}^{[2]\top} & 0 & -\mathcal{J}_{23}^{[2]\top} & 0 & \mathcal{J}_{33}^{[2]} \end{bmatrix}, \quad \mathcal{B} := \begin{bmatrix} \mathcal{B}_1^{[1]} & 0 \\ 0 & \mathcal{B}_1^{[2]} \\ \mathcal{B}_2^{[1]} & 0 \\ 0 & \mathcal{B}_2^{[2]} \\ \mathcal{B}_3^{[1]} & 0 \\ 0 & \mathcal{B}_3^{[2]} \end{bmatrix},$$

and  $\mathcal{R}$  correspondingly. Since  $\mathcal{J}^{[i]}$  is skew-symmetric, so are  $\mathcal{J}_{11}^{[i]}$ ,  $\mathcal{J}_{22}^{[i]}$  and  $\mathcal{J}_{33}^{[i]}$  for  $i = 1, 2$ . Hence,  $\mathcal{J}$  is skew-symmetric. Similarly, it can be shown that  $\mathcal{R}$  is symmetric and positive semi-definite. The two output equations can be combined to

$$\mathbf{y} = \begin{bmatrix} \mathbf{y}^{[1]} \\ \mathbf{y}^{[2]} \end{bmatrix} = \mathcal{B}^\top \begin{bmatrix} \frac{d}{dt} \mathbf{z}_1 \\ \mathbf{e}(\mathbf{z}_1, \mathbf{z}_2) \\ \mathbf{z}_3 \end{bmatrix}, \quad \mathbf{e}(\mathbf{z}_1, \mathbf{z}_2) = \begin{bmatrix} \mathbf{e}^{[1]}(\mathbf{z}_1^{[1]}, \mathbf{z}_2^{[1]}) \\ \mathbf{e}^{[2]}(\mathbf{z}_1^{[2]}, \mathbf{z}_2^{[2]}) \end{bmatrix}.$$

With  $\mathcal{E} := \text{Diag}(\mathcal{E}^{[1]}, \mathcal{E}^{[2]})$ , the efforts satisfy

$$\mathcal{E}^\top \mathbf{e}(\mathbf{z}_1, \mathbf{z}_2) = \begin{bmatrix} \mathcal{E}^{[1]\top} \mathbf{e}^{[1]}(\mathbf{z}_1^{[1]}, \mathbf{z}_2^{[1]}) \\ \mathcal{E}^{[2]\top} \mathbf{e}^{[2]}(\mathbf{z}_1^{[2]}, \mathbf{z}_2^{[2]}) \end{bmatrix} = \begin{bmatrix} \partial_2 \mathcal{H}^{[1]} \\ \partial_2 \mathcal{H}^{[2]} \end{bmatrix} = \nabla_{\mathbf{z}_2} \mathcal{H}.$$

Together with the interconnection equation, namely  $\mathbf{u} = (\mathcal{F}_{\text{skew}} - \mathcal{F}_{\text{sym}}) \mathbf{y} + \tilde{\mathbf{u}}$ ,

we get

$$\begin{aligned} \begin{bmatrix} \nabla_{z_1} \mathcal{H} \\ \mathcal{E} \frac{d}{dt} z_2 \\ 0 \end{bmatrix} &= (\mathcal{J} - \mathcal{R}) \begin{bmatrix} \frac{d}{dt} z_1 \\ e(z_1, z_2) \\ z_3 \end{bmatrix} + \mathcal{B} (\mathcal{F}_{\text{skew}} - \mathcal{F}_{\text{sym}}) \mathbf{y} + \mathcal{B} \tilde{\mathbf{u}} \\ &= \left( (\mathcal{J} + \mathcal{B} \mathcal{F}_{\text{skew}} \mathcal{B}^\top) - (\mathcal{R} + \mathcal{B} \mathcal{F}_{\text{sym}} \mathcal{B}^\top) \right) \begin{bmatrix} \frac{d}{dt} z_1 \\ e(z_1, z_2) \\ z_3 \end{bmatrix} + \mathcal{B} \tilde{\mathbf{u}}, \end{aligned}$$

which has the form (1). To see this, note that  $\mathcal{B} \mathcal{F}_{\text{skew}} \mathcal{B}^\top$  is skew-symmetric and  $\mathcal{B} \mathcal{F}_{\text{sym}} \mathcal{B}^\top$  symmetric positive semi-definite.  $\square$

## 2.2. Time Discretization by the Midpoint Rule

We consider an equidistant partition of the time interval with step size  $\tau$  and  $t_0 = 0$ . As usual,  $x^k$  denotes the approximation of some variable  $x$  at time  $t_k := k\tau$ . Moreover, we use the notation  $x^{k+1/2} = \frac{1}{2}(x^k + x^{k+1})$  and  $\mathbf{u}^{k+1/2} = \mathbf{u}(t^{k+1/2})$  for the input.

**Lemma 4** (Discrete energy dissipation). *Let the Hamiltonian be of the quadratic form*

$$\mathcal{H}(z_1, z_2) = \frac{1}{2} \langle z_1, \mathcal{M}_1 z_1 \rangle + \frac{1}{2} \langle z_2, \mathcal{M}_2 z_2 \rangle$$

with symmetric matrices  $\mathcal{M}_1 \in \mathbb{R}^{n_1 \times n_1}$  and  $\mathcal{M}_2 \in \mathbb{R}^{n_2 \times n_2}$ . With the discrete energy  $\mathcal{H}^k := \mathcal{H}(z_1^k, z_2^k)$ , the midpoint scheme applied to (1) satisfies

$$\mathcal{H}^{k+1} - \mathcal{H}^k \leq \tau \langle \mathbf{y}^{k+1/2}, \mathbf{u}^{k+1/2} \rangle.$$

In particular, we have  $\mathcal{H}^{k+1} \leq \mathcal{H}^k$  for  $\mathbf{u} = 0$ .

*Proof.* The midpoint rule applied to (1) results in the iteration

$$\begin{bmatrix} \tau \nabla_{z_1} \mathcal{H}^{k+1/2} \\ \mathcal{E} (z_2^{k+1} - z_2^k) \\ 0 \end{bmatrix} = (\mathcal{J} - \mathcal{R}) \begin{bmatrix} z_1^{k+1} - z_1^k \\ \tau e(z_1^{k+1/2}, z_2^{k+1/2}) \\ \tau z_3^{k+1/2} \end{bmatrix} + \tau \mathcal{B} \mathbf{u}^{k+1/2}, \quad (4a)$$

$$\tau \mathbf{y}^{k+1/2} = \mathcal{B}^\top \begin{bmatrix} z_1^{k+1} - z_1^k \\ \tau e(z_1^{k+1/2}, z_2^{k+1/2}) \\ \tau z_3^{k+1/2} \end{bmatrix}. \quad (4b)$$

Since the Hamiltonian is quadratic, we have  $\nabla_{z_\ell} \mathcal{H}^k = \mathcal{M}_\ell z_\ell^k$ ,  $\ell = 1, 2$ . This implies

$$\mathcal{E}^\top \mathbf{e}(z_1^{k+1/2}, z_2^{k+1/2}) = \nabla_{z_2} \mathcal{H}(z_1^{k+1/2}, z_2^{k+1/2}) = \nabla_{z_2} \mathcal{H}^{k+1/2}$$

as well as

$$2\mathcal{H}^k = \langle z_1^k, \mathcal{M}_1 z_1^k \rangle + \langle z_2^k, \mathcal{M}_2 z_2^k \rangle = \langle z^k, \nabla_z \mathcal{H}^k \rangle.$$

Due to the symmetry of  $\mathcal{M}_1$  and  $\mathcal{M}_2$ , we conclude that

$$2\mathcal{H}^{k+1} - 2\mathcal{H}^k = \langle z^{k+1}, \nabla_z \mathcal{H}^{k+1} \rangle - \langle z^k, \nabla_z \mathcal{H}^k \rangle = 2 \langle z^{k+1} - z^k, \partial_z \mathcal{H}^{k+1/2} \rangle.$$

Hence,

$$\begin{aligned} \tau (\mathcal{H}^{k+1} - \mathcal{H}^k) &= \tau \langle z^{k+1} - z^k, \partial_z \mathcal{H}^{k+1/2} \rangle \\ &= \left\langle \begin{bmatrix} z_1^{k+1} - z_1^k \\ \tau \nabla_{z_2} \mathcal{H}^{k+1/2} \\ \tau z_3^{k+1/2} \end{bmatrix}, \begin{bmatrix} \tau \nabla_{z_1} \mathcal{H}^{k+1/2} \\ z_2^{k+1} - z_2^k \\ 0 \end{bmatrix} \right\rangle \\ &= \left\langle \begin{bmatrix} z_1^{k+1} - z_1^k \\ \tau \mathbf{e}(z_1^{k+1/2}, z_2^{k+1/2}) \\ \tau z_3^{k+1/2} \end{bmatrix}, \begin{bmatrix} \tau \nabla_{z_1} \mathcal{H}^{k+1/2} \\ \mathcal{E}(z_2^{k+1} - z_2^k) \\ 0 \end{bmatrix} \right\rangle. \end{aligned}$$

Inserting (4) finally gives

$$\begin{aligned} \tau (\mathcal{H}^{k+1} - \mathcal{H}^k) &\leq \left\langle \begin{bmatrix} z_1^{k+1} - z_1^k \\ \tau \mathbf{e}(z_1^{k+1/2}, z_2^{k+1/2}) \\ \tau z_3^{k+1/2} \end{bmatrix}, \tau \mathcal{B} \mathbf{u}^{k+1/2} \right\rangle \\ &= \tau^2 \langle \mathbf{y}^{k+1/2}, \mathbf{u}^{k+1/2} \rangle. \quad \square \end{aligned}$$

**Remark 5.** For linear time-invariant systems, the midpoint rule and the trapezoidal rule coincide. Hence, also the trapezoidal rule conserves the energy dissipation for this kind of systems, cf. the numerical experiments in Section 4.

### 3. Conductor Models

In low-frequency numerical computations of electromagnetic fields, so-called conductor models are used to couple conducting regions, e.g., coils, to outside circuitry [31]. Three conductor models are commonly distinguished:

stranded, solid, and foil conductors, [32, 33, 34, 37]. We consider the conductor models in the magnetoquasistatic regime of Maxwell's equations, i.e., disregarding displacement currents [38]. For that, we choose the (modified) vector potential formulation using  $\vec{A}: \Omega \times [t_0, t_f] \rightarrow \mathbb{R}^3$  as the main unknown, see [39]. Imposing homogeneous Dirichlet boundary conditions for simplicity of presentation, this leads to the so-called eddy current problem

$$\begin{aligned} \nabla \times (\nu \nabla \times \vec{A}) &= \vec{J} && \text{in } \Omega, \\ \vec{n} \times \vec{A} &= 0 && \text{on } \partial\Omega, \end{aligned}$$

where  $\vec{n}$  denotes the outward pointing normal vector,  $\nu$  is the magnetic permeability, and  $\vec{J}: \Omega \times [t_0, t_f] \rightarrow \mathbb{R}^3$  equals the total current density. Again, for simplicity, we restrict ourselves to a linear isotropic reluctivity  $\nu \in \mathbb{R}_{>0}$ . The total current density is split into

$$\vec{J} = \vec{J}_c + \vec{J}_s,$$

where  $\vec{J}_c$  is the conduction current density, accounting for the ohmic losses, and  $\vec{J}_s$  the source current density. The conduction current density is given by Ohm's law  $\vec{J}_c = -\sigma \partial_t \vec{A}$ , where  $-\partial_t \vec{A}$  is the electric field strength, and in which the electric conductivity may jump

$$\sigma = \begin{cases} \sigma_c & \text{in } \Omega_c \subset \Omega \\ 0 & \text{otherwise} \end{cases}$$

with  $\sigma_c \in \mathbb{R}_{>0}$ . Then, the parabolic semi-elliptic curl-curl equation can be written as

$$\sigma \partial_t \vec{A} + \nabla \times (\nu \nabla \times \vec{A}) = \vec{J}_s \quad \text{in } \Omega, \quad (5)$$

$$\vec{n} \times \vec{A} = 0 \quad \text{on } \partial\Omega \quad (6)$$

with a given (consistent) initial condition  $\vec{A}(\vec{x}, 0) = \vec{A}_0(\vec{x})$  for  $\vec{x} \in \Omega$ . Note that (5) does not define  $\vec{A}$  uniquely in non-conducting domains due to gradient fields spanning the nullspace of the curl operator [38]. There are different choices to deal with the non-uniqueness and we will follow the tree-cotree approach from [40].

To discuss the conductor models giving rise to the source current density  $\vec{J}_s$ , we consider Fig. 1. It implicitly encodes the following assumptions from [37].

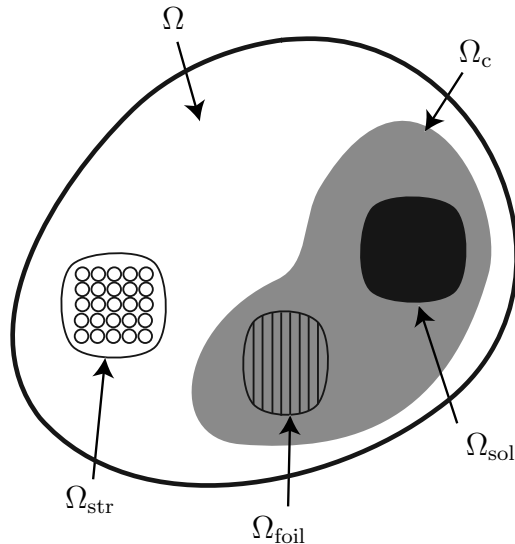


Figure 1: Computational domain with one representative of each conductor model.

**Assumption 1** (Domain).  $\Omega$  is simply connected and split into two disjoint subdomains  $\Omega_c$  and  $\Omega_0$  related to the conductivity, i.e.,  $\bar{\Omega} = \bar{\Omega}_c \cup \bar{\Omega}_0$ . Furthermore, there is a source domain  $\Omega_s \subset \Omega$ , with  $\text{supp}(\vec{J}_s) = \Omega_s$ , which can be divided into three disjoint subdomains  $\Omega_s = \Omega_{sol} \cup \Omega_{foil} \cup \Omega_{str}$ , corresponding to solid, foil, and stranded conductors, respectively. The source subdomains satisfy  $\Omega_{sol}, \Omega_{foil} \subset \Omega_c$  and  $\Omega_{str} \subset \Omega_0$ . Note that these domains related to conductors may appear  $n_{str}$ ,  $n_{sol}$  and  $n_{foil}$  times. Finally, we assume that all domains are Lipschitz, open, and – where applicable – their closures do not intersect, e.g.,  $\bar{\Omega}_{sol} \cap \bar{\Omega}_{foil} = \emptyset$ .

A mimetic finite element (FE) discretization of (5) requires specific function spaces spanned by so-called edge-elements basis functions which is well understood, see e.g. [41]. Without introducing the corresponding function spaces or basis construction, we directly state the result of semi-discretization by the Galerkin method

$$\mathbf{M}_\sigma \frac{d}{dt} \mathbf{a}(t) + \mathbf{K}_\nu \mathbf{a}(t) = \mathbf{j}_s(t), \quad (7)$$

where  $\mathbf{a}: [t_0, t_f] \rightarrow \mathbb{R}^{n_w}$  contains the FEM coefficients of the magnetic vector potential  $\vec{A}$  and  $\mathbf{j}_s$  is the discretized source current density which will be discussed in detail in the upcoming subsections. The  $i$ th basis function for

$\vec{A}$  is denoted as  $\vec{w}_i$ , and the FE matrices  $\mathbf{M}_\sigma, \mathbf{K}_\nu \in \mathbb{R}^{n_w \times n_w}$  and  $\mathbf{j}_s \in \mathbb{R}^{n_w}$  are defined as

$$[\mathbf{M}_\sigma]_{ij} = \int_{\Omega} \sigma \vec{w}_j \cdot \vec{w}_i \, dV, \quad (8)$$

$$[\mathbf{K}_\nu]_{ij} = \int_{\Omega} \nu \nabla \times \vec{w}_j \cdot \nabla \times \vec{w}_i \, dV, \quad (9)$$

$$[\mathbf{j}_s]_i = \int_{\Omega} \vec{J}_s \cdot \vec{w}_i \, dV. \quad (10)$$

Note that (7) is a DAE due to the singularity of the conductivity matrix [42].

**Property 6** (System matrices). *The conductivity matrix  $\mathbf{M}_\sigma$  and the reluctance matrix  $\mathbf{K}_\nu$  are positive semi-definite.*

*Proof.* This follows immediately from the Galerkin discretization in (8)-(9) and the non-negativity of the material properties.  $\square$

The non-uniqueness of the continuous formulation is inherited by the discrete one, i.e., there is a joint nullspace of  $\mathbf{M}_\sigma$  and  $\mathbf{K}_\nu$ . However, this can be removed by gauging, in particular the tree-cotree approach; see [43, p. 58].

**Assumption 2** (Uniqueness). *We assume that a tree-cotree gauging has been applied such that the matrix pencil  $\lambda \mathbf{M}_\sigma + \mathbf{K}_\nu$  with  $\lambda \in \mathbb{R}$  is regular, and (7) has a unique solution given a consistent initial value  $\mathbf{a}(t_0) = \mathbf{a}_0 \in \mathbb{R}^{n_w}$ .*

### 3.1. Stranded Conductor

The stranded conductor is a simple homogenization model that avoids resolving single strands by considering a bulk material. This is a reasonable assumption if their radius is significantly below the skin depth such that eddy current effects are negligible [31]. For multiple conductors of this type, the source current density has only support in  $\Omega_s = \bigcup_{k=1}^{n_{\text{str}}} \Omega_{\text{str},k}$  and  $\Omega_{\text{sol}} = \Omega_{\text{foil}} = \emptyset$ . The model is based on distribution functions  $\vec{\chi}_{\text{str},k} : \Omega_{\text{str},k} \rightarrow \mathbb{R}^3$ , called winding function in [33] where

$$\vec{J}_s = \sum_k^{n_{\text{str}}} \vec{\chi}_{\text{str},k} \iota_{\text{str},k}$$

with  $\mathbf{z}_{\text{str}}: [t_0, t_f] \rightarrow \mathbb{R}^{n_{\text{str}}}$ . Each winding function can be discretized as described in (10) and collected in  $\mathbf{X}_{\text{str}} \in \mathbb{R}^{n_w \times n_{\text{str}}}$ . Then, this matrix can also be used to express the voltage drops  $\mathbf{v}_{\text{str}}: [t_0, t_f] \rightarrow \mathbb{R}^{n_{\text{str}}}$  such that the resulting system reads [33]

$$\mathbf{M}_\sigma \frac{d}{dt} \mathbf{a} + \mathbf{K}_\nu \mathbf{a} - \mathbf{X}_{\text{str}} \mathbf{z}_{\text{str}} = 0, \quad (11a)$$

$$\mathbf{X}_{\text{str}}^\top \frac{d}{dt} \mathbf{a} + \mathbf{R}_{\text{str}} \mathbf{z}_{\text{str}} - \mathbf{v}_{\text{str}} = 0, \quad (11b)$$

where the resistance is given by

$$\mathbf{R}_{\text{str}} = \mathbf{X}_{\text{str}}^\top \mathbf{M}_{\text{str}}^+ \mathbf{X}_{\text{str}}$$

with the Moore–Penrose pseudo-inverse  $\mathbf{M}_{\text{str}}^+$  of  $\mathbf{M}_{\text{str}}$ , which is built analogously to (8) by adding a conductivity  $\sigma = \sigma_{\text{str}} > 0$  on the stranded conductor domain  $\Omega_{\text{str}}$ . This accounts for losses due to direct currents, while eddy currents are still neglected.

**Property 7.** *The resistance matrix  $\mathbf{R}_{\text{str}}$  is positive semi-definite.*

*Proof.* Due to its construction and the fact that  $\sigma_{\text{str}} > 0$ ,  $\mathbf{M}_{\text{str}}$  is positive semi-definite and so is  $\mathbf{M}_{\text{str}}^+$ .  $\square$

In practice,  $\mathbf{R}_{\text{str}}$  is positive definite. This can also be proven by exploiting additional properties of the winding functions. However, we only need semi-definiteness for the following result

**Lemma 8.** *The stranded conductor model (11) fits into the structure (3).*

*Proof.* We set  $\mathbf{z}_1 = \mathbf{a}$ ,  $\mathbf{z}_3 = \mathbf{z}_{\text{str}}$ ,  $\mathcal{H}(\mathbf{a}) = \frac{1}{2} \mathbf{a}^\top \mathbf{K}_\nu \mathbf{a}$ ,  $\mathbf{u} = \mathbf{v}_{\text{str}}$ , and

$$\mathcal{J} = \begin{bmatrix} 0 & \mathbf{X}_{\text{str}} \\ -\mathbf{X}_{\text{str}}^\top & 0 \end{bmatrix}, \quad \mathcal{R} = \begin{bmatrix} \mathbf{M}_\sigma & 0 \\ 0 & \mathbf{R}_{\text{str}} \end{bmatrix}, \quad \mathcal{B} = \begin{bmatrix} 0 \\ \mathbf{I} \end{bmatrix},$$

where  $\mathbf{I}$  denotes the identity and  $\mathbf{M}_\sigma$  and  $\mathbf{R}_{\text{str}}$  are positive semi-definite.  $\square$

Note that all terms in  $\mathcal{R}$  are indeed related to conductivity or resistivity. The resulting power balance reads

$$\frac{d}{dt} \mathcal{H}(\mathbf{a}) = - \begin{bmatrix} \frac{d}{dt} \mathbf{a} \\ \mathbf{z}_{\text{str}} \end{bmatrix}^\top \begin{bmatrix} \mathbf{M}_\sigma & 0 \\ 0 & \mathbf{R}_{\text{str}} \end{bmatrix} \begin{bmatrix} \frac{d}{dt} \mathbf{a} \\ \mathbf{z}_{\text{str}} \end{bmatrix} + \mathbf{z}_{\text{str}} \cdot \mathbf{v}_{\text{str}}.$$

### 3.2. Solid Conductor

If eddy currents are non-negligible in a conductor, the solid conductor model is used. Let us assume multiple conductors of this type, then the source current density has support in  $\Omega_s = \bigcup_{k=1}^{n_{\text{sol}}} \Omega_{\text{sol},k}$  and  $\Omega_{\text{str}} = \Omega_{\text{foil}} = \emptyset$ . The coupling is established by voltage distribution functions such that

$$\vec{J}_s = \sum_k^{n_{\text{sol}}} \sigma \vec{\chi}_{\text{sol},k} v_{\text{sol},k}$$

with voltages  $\mathbf{v}_{\text{sol}}: [t_0, t_f] \rightarrow \mathbb{R}^{n_{\text{sol}}}$ . Again, each distribution function  $\vec{\chi}_{\text{sol},k}: \Omega_{\text{sol},k} \rightarrow \mathbb{R}^3$  can be discretized separately and collected in a matrix  $\mathbf{X}_{\text{sol}} \in \mathbb{R}^{n_w \times n_{\text{sol}}}$  such that the system reads

$$\mathbf{M}_\sigma \frac{d}{dt} \mathbf{a} + \mathbf{K}_\nu \mathbf{a} - \mathbf{M}_\sigma \mathbf{X}_{\text{sol}} \mathbf{v}_{\text{sol}} = 0, \quad (12a)$$

$$-\mathbf{X}_{\text{sol}}^\top \mathbf{M}_\sigma^\top \frac{d}{dt} \mathbf{a} + \mathbf{G}_{\text{sol}} \mathbf{v}_{\text{sol}} - \mathbf{v}_{\text{sol}} = 0 \quad (12b)$$

with  $\mathbf{v}_{\text{sol}}: [t_0, t_f] \rightarrow \mathbb{R}^{n_{\text{sol}}}$ . The (direct current) conductance matrix is defined as

$$\mathbf{G}_{\text{sol}} = \mathbf{X}_{\text{sol}}^\top \mathbf{M}_\sigma \mathbf{X}_{\text{sol}}. \quad (13)$$

**Property 9.** *The conductance matrix  $\mathbf{G}_{\text{sol}}$  is positive semi-definite.*

*Proof.* This follows immediately from the positive semi-definiteness of (8).  $\square$

Note that one can show again the stronger result of positive definiteness if considering the exact images and spaces of the involved matrices. However, semi-definiteness is enough to prove the following result.

**Lemma 10.** *The solid conductor model (12) fits into the structure (3).*

*Proof.* We define  $\mathbf{z}_1 = \mathbf{a}$ ,  $\mathbf{z}_3 = \mathbf{v}_{\text{sol}}$ ,  $\mathcal{H}(\mathbf{a}) = \frac{1}{2} \mathbf{a}^\top \mathbf{K}_\nu \mathbf{a}$ ,  $\mathbf{u} = \mathbf{v}_{\text{sol}}$ , and

$$\mathcal{J} = 0, \quad \mathcal{R} = \begin{bmatrix} \mathbf{M}_\sigma & -\mathbf{M}_\sigma \mathbf{X}_{\text{sol}} \\ -\mathbf{X}_{\text{sol}}^\top \mathbf{M}_\sigma^\top & \mathbf{G}_{\text{sol}} \end{bmatrix}, \quad \mathcal{B} = \begin{bmatrix} 0 \\ \mathbf{I} \end{bmatrix}$$

with identity  $\mathbf{I}$ . Using (13), we observe that  $\mathcal{R}$  may be factorized as

$$\mathcal{R} = [\mathbf{I} \quad -\mathbf{X}_{\text{sol}}]^\top \mathbf{M}_\sigma [\mathbf{I} \quad -\mathbf{X}_{\text{sol}}]$$

and thus  $\mathcal{R}$  inherits the positive semi-definiteness from  $\mathbf{M}_\sigma$ , cf. Property 6.  $\square$

Note, all terms in  $\mathcal{R}$  are again related to conductivity or resistivity. The power balance reads

$$\frac{d}{dt}\mathcal{H}(\mathbf{a}) = - \begin{bmatrix} \frac{d}{dt}\mathbf{a} \\ \mathbf{v}_{\text{sol}} \end{bmatrix}^\top \begin{bmatrix} \mathbf{M}_\sigma & -\mathbf{M}_\sigma\mathbf{X}_{\text{sol}} \\ -\mathbf{X}_{\text{sol}}^\top\mathbf{M}_\sigma^\top & \mathbf{G}_{\text{sol}} \end{bmatrix} \begin{bmatrix} \frac{d}{dt}\mathbf{a} \\ \mathbf{v}_{\text{sol}} \end{bmatrix} + \mathbf{v}_{\text{sol}} \cdot \mathbf{v}_{\text{sol}}.$$

### 3.3. Foil Conductor

The foil conductor is represented by a homogenization model that lies, in a sense, between the solid and stranded types. It captures eddy currents within the foils but neglects them in the perpendicular direction [32, 44]. The following discussion is based on [34], to which we refer for more details. Since the model already resolves several foils, we present here the simplified case of a single conductor to avoid confusion, i.e.,  $\Omega_s = \Omega_{\text{foil}}$ . The source current density is written as

$$\vec{J}_s = \sigma\Phi\vec{\chi}_{\text{sol}},$$

where the electric field is expressed in terms of a voltage function  $\Phi: \Omega \times [t_0, t_f] \rightarrow \mathbb{R}$  and a distribution function  $\vec{\chi}_{\text{sol}}$ . By imposing the same current  $i_{\text{foil}}$  through every (virtual) foil, it can be expressed in the homogenized region as

$$\int_{\Gamma(\alpha)} \sigma \left( -\partial_t \vec{A} + \Phi \vec{\chi}_{\text{sol}} \right) \cdot \vec{\chi}_{\text{sol}} dS = \frac{i_{\text{foil}}}{b}, \quad (14)$$

where  $b$  is the thickness of a foil and  $\Gamma(\alpha)$  defines a surface perpendicular to the thickness in  $\Omega_{\text{foil}}$ . The voltage over the foil winding  $v_{\text{foil}}$  is the sum of the voltage drops of the individual foils, which is expressed for the homogenized domain as

$$v_{\text{foil}} = \frac{1}{b} \int_{\mathbf{f}(L_\alpha, \beta, \gamma)} \Phi ds, \quad (15)$$

where  $\mathbf{f}(L_\alpha, \beta, \gamma)$  is the one-dimensional domain of homogenization of the foil conductor. Finally, the FE discretization of (7), (14), and (15) yields a system of equations

$$\mathbf{M}_\sigma \frac{d}{dt}\mathbf{a} + \mathbf{K}_\nu \mathbf{a} - \mathbf{X}_{\text{foil}} \mathbf{e} = 0, \quad (16a)$$

$$-\mathbf{X}_{\text{foil}}^\top \frac{d}{dt}\mathbf{a} + \mathbf{G}_{\text{foil}} \mathbf{e} - \mathbf{c}i_{\text{foil}} = 0, \quad (16b)$$

$$-\mathbf{c}^\top \mathbf{e} + v_{\text{foil}} = 0, \quad (16c)$$

where  $\mathbf{e}: [t_0, t_f] \rightarrow \mathbb{R}^{n_p}$  contains the FEM coefficients of the electric scalar potential, and the matrix  $\mathbf{X}_{\text{foil}} \in \mathbb{R}^{n_w \times n_p}$  and the vector  $\mathbf{c} \in \mathbb{R}^{n_p}$  are defined by

$$[\mathbf{X}_{\text{foil}}]_{i\ell} = \sum_{j=1}^{n_w} x_j \int_{\Omega} \sigma p_{\ell} \vec{w}_j \cdot \vec{w}_i \, dV,$$

$$[\mathbf{c}]_k = \frac{1}{b} \int_{\mathbf{f}(L_{\alpha, \beta, \gamma})} p_k \, ds.$$

Here,  $p_k$ ,  $k = 1, \dots, n_p$ , denote the FEM basis functions for the discretization of  $\Phi$ , which can be defined independently of the underlying mesh. Moreover, the vector  $\mathbf{x} = [x_1, \dots, x_{n_w}]^{\top}$  contains the coordinates of  $\vec{\chi}_{\text{sol}}$  w.r.t. the basis  $(\vec{w}_i)_{i=1}^{n_w}$ . The conductance matrix  $\mathbf{G}_{\text{foil}} \in \mathbb{R}^{n_p \times n_p}$  is defined as

$$\mathbf{G}_{\text{foil}} = \mathbf{X}_{\text{foil}}^{\top} \mathbf{M}_{\sigma}^{+} \mathbf{X}_{\text{foil}}$$

where  $\mathbf{M}_{\sigma}^{+}$  is the Moore–Penrose pseudo-inverse of  $\mathbf{M}_{\sigma}$ .

**Property 11.** *The conductance matrix  $\mathbf{G}_{\text{foil}}$  is positive semi-definite.*

*Proof.* This follows again from the positive semi-definiteness of (8).  $\square$

Our definition of  $\mathbf{G}_{\text{foil}}$  ensures consistency with circuit theory, as is discussed in [34]. However, the legacy definition from the literature also fulfills the relevant properties to prove the following Lemma. Note that in the specific case of discretizing  $\Phi$  with  $n_p = 1$  basis function  $p_1 = 1$ , the foil conductor model becomes equivalent with the solid conductor model.

**Lemma 12.** *The foil conductor model (16) fits into the structure (3).*

*Proof.* We define  $\mathbf{z}_1 = \mathbf{a}$ ,  $\mathbf{z}_3 = [\mathbf{e}^{\top} \ \nu_{\text{foil}}]^{\top}$ ,  $\mathcal{H}(\mathbf{a}) = \frac{1}{2} \mathbf{a}^{\top} \mathbf{K}_{\nu} \mathbf{a}$ ,  $\mathbf{u} = \nu_{\text{foil}}$ , and

$$\mathcal{J} = \begin{bmatrix} 0 & 0 & 0 \\ 0 & 0 & \mathbf{c} \\ 0 & -\mathbf{c}^{\top} & 0 \end{bmatrix}, \quad \mathcal{R} = \begin{bmatrix} \mathbf{M}_{\sigma} & -\mathbf{X}_{\text{foil}} & 0 \\ -\mathbf{X}_{\text{foil}}^{\top} & \mathbf{G}_{\text{foil}} & 0 \\ 0 & 0 & 0 \end{bmatrix}, \quad \mathcal{B} = \begin{bmatrix} 0 \\ 0 \\ 1 \end{bmatrix}.$$

It remains to be shown that  $\mathcal{R}$  is positive semi-definite. We use [45, Th. 1.20] which states that this is equivalent to

- (i) the matrix  $\mathbf{M}_{\sigma}$  is positive semi-definite,

(ii) the column spaces match, i.e.,  $C(\mathbf{X}_{\text{foil}}) \subseteq C(\mathbf{M}_\sigma)$ ,

(iii) the Schur complement  $\mathbf{G}_{\text{foil}} - \mathbf{X}_{\text{foil}}^\top \mathbf{M}_\sigma^+ \mathbf{X}_{\text{foil}}$  is positive semi-definite.

Since (i) and (iii) follow directly from the definitions, we only need to show (ii). For this, we denote the projector onto the nullspace of  $\mathbf{M}_\sigma$  by  $\mathbf{Q}_\sigma$ . It is easy to show that  $\mathbf{Q}_\sigma \mathbf{X}_{\text{foil}} = 0$ , see [34, App. II] which gives (ii) and thus concludes the proof.  $\square$

The power balance reads

$$\frac{d}{dt} \mathcal{H}(\mathbf{a}) = - \begin{bmatrix} \frac{d}{dt} \mathbf{a} \\ \mathbf{e} \end{bmatrix}^\top \begin{bmatrix} \mathbf{M}_\sigma & -\mathbf{X}_{\text{foil}} \\ -\mathbf{X}_{\text{foil}}^\top & \mathbf{G}_{\text{foil}} \end{bmatrix} \begin{bmatrix} \frac{d}{dt} \mathbf{a} \\ \mathbf{e} \end{bmatrix} + \iota_{\text{foil}} \nu_{\text{foil}}.$$

### 3.4. Field Circuit Coupling using MNA

There are various formulations to describe electric circuits, however, the arguably most successful is the MNA [46]. Using the notation from [35], the dynamics of a linear circuit are then described by the governing equations

$$\mathbf{A}_C \mathbf{C} \mathbf{A}_C^\top \frac{d}{dt} \boldsymbol{\phi} + \mathbf{A}_R \mathbf{G} \mathbf{A}_R^\top \boldsymbol{\phi} + \mathbf{A}_L \mathbf{j}_L + \mathbf{A}_V \mathbf{j}_V + \mathbf{A}_I \boldsymbol{\iota} = 0, \quad (17a)$$

$$\mathbf{L} \frac{d}{dt} \mathbf{j}_L - \mathbf{A}_L^\top \boldsymbol{\phi} = 0, \quad (17b)$$

$$\mathbf{A}_V^\top \boldsymbol{\phi} - \mathbf{v} = 0, \quad (17c)$$

where  $\mathbf{A}_\star \in \mathbb{R}^{(n_\phi-1) \times b_\star}$  are incidence matrices,  $\boldsymbol{\iota}: [t_0, t_f] \rightarrow \mathbb{R}^{b_I}$  the source currents and  $\mathbf{v}: [t_0, t_f] \rightarrow \mathbb{R}^{b_V}$  the source voltages. The number of nodes in the circuit is denoted as  $n_\phi$  and  $b_\star$  is the number of (branches containing) the examined circuit element. The system unknowns are the node potentials  $\boldsymbol{\phi}: [t_0, t_f] \rightarrow \mathbb{R}^{n_\phi-1}$ , currents through inductances  $\mathbf{j}_L: [t_0, t_f] \rightarrow \mathbb{R}^{b_L}$ , and currents through voltage sources  $\mathbf{j}_V: [t_0, t_f] \rightarrow \mathbb{R}^{b_V}$ .

The matrices of conductances  $\mathbf{G} \in \mathbb{R}^{b_R \times b_R}$ , inductances  $\mathbf{L} \in \mathbb{R}^{b_L \times b_L}$  and capacitances  $\mathbf{C} \in \mathbb{R}^{b_C \times b_C}$  are symmetric and positive definite, whereas  $\mathbf{A}_C$  does not necessarily have full row rank [35]. As a consequence, the matrix  $\mathbf{A}_C \mathbf{C} \mathbf{A}_C^\top$  may, in general, be singular and the problem is of differential-algebraic nature. It is known to have a (differential) index of up to two for specific circuit configurations. Nonetheless, we can show the following result.

**Lemma 13.** *The MNA model (17) fits into the structure (1).*

*Proof.* We set

$$\mathbf{z}_2 = \begin{bmatrix} \boldsymbol{\phi} \\ \mathbf{J}_L \end{bmatrix} = \mathbf{e}(\mathbf{z}_2), \quad \mathbf{z}_3 = \mathbf{J}_V, \quad \mathbf{u} = \begin{bmatrix} \mathbf{i} \\ \mathbf{v} \end{bmatrix}$$

and consider the energy  $\mathcal{H}(\mathbf{z}_2) = \frac{1}{2} \boldsymbol{\phi}^\top \mathbf{A}_C \mathbf{C} \mathbf{A}_C^\top \boldsymbol{\phi} + \frac{1}{2} \mathbf{J}_L^\top \mathbf{L} \mathbf{J}_L$ . Then the choices

$$\begin{aligned} \mathcal{E} &= \begin{bmatrix} \mathbf{A}_C \mathbf{C} \mathbf{A}_C^\top & 0 \\ 0 & \mathbf{L} \end{bmatrix}, & \mathcal{J} &= \begin{bmatrix} 0 & -\mathbf{A}_L & -\mathbf{A}_V \\ \mathbf{A}_L^\top & 0 & 0 \\ \mathbf{A}_V^\top & 0 & 0 \end{bmatrix}, \\ \mathcal{R} &= \begin{bmatrix} \mathbf{A}_R \mathbf{G} \mathbf{A}_R^\top & 0 & 0 \\ 0 & 0 & 0 \\ 0 & 0 & 0 \end{bmatrix}, & \mathcal{B} &= - \begin{bmatrix} \mathbf{A}_I & 0 \\ 0 & 0 \\ 0 & I \end{bmatrix} \end{aligned}$$

satisfy

$$\mathcal{E}^\top \mathbf{e}(\mathbf{z}_2) = \begin{bmatrix} \mathbf{A}_C \mathbf{C} \mathbf{A}_C^\top & 0 \\ 0 & \mathbf{L} \end{bmatrix} \mathbf{z}_2 = \begin{bmatrix} \mathbf{A}_C \mathbf{C} \mathbf{A}_C^\top \boldsymbol{\phi} \\ \mathbf{L} \mathbf{J}_L \end{bmatrix} = \nabla_{\mathbf{z}_2} \mathcal{H}(\mathbf{z}_2)$$

with  $\mathcal{R}$  being again positive semi-definite.  $\square$

Let us exploit the structure-preserving interconnection property from Lemma 3. For the coupling of the MNA equations and the conductor models, we define the currents and voltages in the MNA equations (17) as

$$\mathbf{i}^\top = [\mathbf{i}_{\text{str}}^\top \quad i_{\text{foil}} \quad \mathbf{i}_{\text{src}}^\top], \quad \mathbf{v}^\top = [\mathbf{v}_{\text{sol}}^\top \quad \mathbf{v}_{\text{src}}^\top], \quad (18)$$

where  $\mathbf{i}_{\text{src}}$  and  $\mathbf{v}_{\text{src}}$  may represent external time-dependent current or voltage sources. For the inputs of the conductor models, we first introduce the splittings

$$\mathbf{A}_I = [\mathbf{A}_{\text{str}} \quad \mathbf{A}_{\text{foil}} \quad \mathbf{A}_{\text{src}}], \quad \mathbf{J}_V^\top = [\mathbf{J}_{\text{sol}}^\top \quad \mathbf{J}_{\text{src}}^\top]$$

according to the splittings of  $\mathbf{i}$  and  $\mathbf{v}$ , respectively, and set

$$\mathbf{i}_{\text{sol}} = \mathbf{J}_{\text{sol}}, \quad \mathbf{v}_{\text{str}} = \mathbf{A}_{\text{str}}^\top \boldsymbol{\phi}, \quad v_{\text{foil}} = \mathbf{A}_{\text{foil}}^\top \boldsymbol{\phi}. \quad (19)$$

In total, the coupling equations (18) and (19) may be summarized as

$$\underbrace{\begin{bmatrix} \iota \\ \mathbf{v} \\ \mathbf{v}_{\text{str}} \\ \iota_{\text{sol}} \\ v_{\text{foil}} \end{bmatrix}}_{=\mathbf{u}} = \underbrace{\begin{bmatrix} 0 & 0 & 0 & 0 & 0 & \mathbf{I} & 0 & 0 \\ 0 & 0 & 0 & 0 & 0 & 0 & 0 & 1 \\ 0 & 0 & 0 & 0 & 0 & 0 & 0 & 0 \\ 0 & 0 & 0 & 0 & 0 & 0 & \mathbf{I} & 0 \\ 0 & 0 & 0 & 0 & 0 & 0 & 0 & 0 \\ -\mathbf{I} & 0 & 0 & 0 & 0 & 0 & 0 & 0 \\ 0 & 0 & 0 & -\mathbf{I} & 0 & 0 & 0 & 0 \\ 0 & -1 & 0 & 0 & 0 & 0 & 0 & 0 \end{bmatrix}}_{=\mathcal{F}_{\text{skew}}} \underbrace{\begin{bmatrix} -\mathbf{A}_{\text{str}}^{\top} \phi \\ -\mathbf{A}_{\text{foil}}^{\top} \phi \\ -\mathbf{A}_{\text{src}}^{\top} \phi \\ -\mathbf{J}_{\text{sol}} \\ -\mathbf{J}_{\text{src}} \\ \iota_{\text{str}} \\ \mathbf{v}_{\text{sol}} \\ \iota_{\text{foil}} \end{bmatrix}}_{=\mathbf{y}} + \underbrace{\begin{bmatrix} 0 \\ 0 \\ \iota_{\text{src}} \\ 0 \\ \mathbf{v}_{\text{src}} \\ 0 \\ 0 \\ 0 \end{bmatrix}}_{=\tilde{\mathbf{u}}}.$$

This is a special case of the structure-preserving interconnection from Lemma 3 and, hence, we obtain the following result.

**Theorem 14.** *The field-circuit coupled model consisting of interconnections of field models (11), (12) and (16) with circuit equations (17) fits into the structure (1).*

#### 4. Numerical Example

This section provides a numerical example of the concepts discussed in the previous sections. We examine an oscillator circuit containing a lumped capacitor and an inductor which embeds a field model. The inductor is modeled with the stranded conductor model (11) in a 2D axisymmetric setting (which requires no gauging). Fig. 2 shows the oscillator circuit and the modeling domain of the field problem. Table 1 lists the parameters of the circuit and the field model. The models were implemented with the open source software GetDP [47] and Gmsh [48].

When there is no resistance in the stranded conductor model and the core is assumed to be nonconducting, the energy in the oscillator circuit is preserved. An energy conserving time integration scheme is required to ensure this property. We use the trapezoidal rule, see Remark 5. As initial conditions, the voltage over the capacitor is set to 1 V and there is no current in the circuit. Fig. 3 shows the oscillation of the energy between the capacitor and the inductor. It is seen how the energy is preserved with the trapezoidal rule whereas implicit Euler is damping the oscillation.

When the core is modeled to be conductive, losses caused by the induced eddy currents are introduced to the system. A conductivity of  $100 \text{ S m}^{-1}$

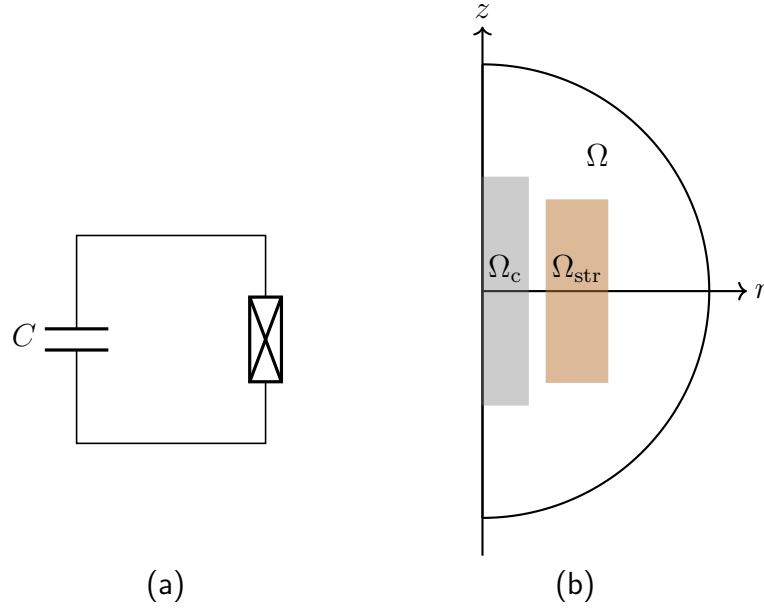


Figure 2: (a) Schematic of the oscillator circuit. (b) 2D axisymmetric modeling domain of the inductor.

Table 1: Parameters of the oscillator example

Quantity	Value
Capacitance	100 $\mu\text{F}$
Core relative permeability	100
Conductor relative permeability	1
Conductor width	25 mm
Conductor height	100 mm
Conductor inner radius	25 mm
Core width	16.7 mm
Core height	120 mm
Time step	0.1 $\mu\text{s}$

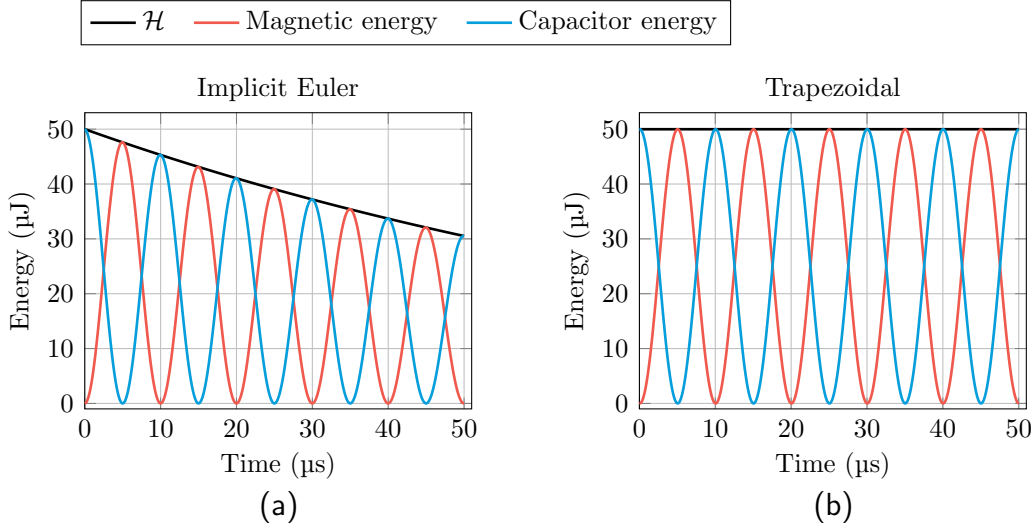


Figure 3: The energy of the oscillator with a nonconducting core when (a) the implicit Euler method and (b) the trapezoidal rule are used for time integration. The Hamiltonian contains the contributions from the magnetic and the capacitor energies.

is assumed in the core region. Fig. 4 shows the oscillation in this slightly modified setting. Now, a damping behavior is observed also with an energy conserving time integrator. However, the additional numerical damping of the implicit Euler method causes a faster damping of the oscillation. When the total dissipated energy is taken into account, it is seen that the energy is still preserved with the trapezoidal rule whereas the implicit Euler method is not able to conserve the energy.

## 5. Summary

The paper develops a unified modeling and discretization framework for coupled field/circuit systems using an energy-based approach inspired by the pH formalism. It builds upon a recent formulation for DAEs, extending it to handle additional algebraic components in the state variables and enabling the structure-preserving interconnection of electric circuits and electromagnetic field models in a consistent framework.

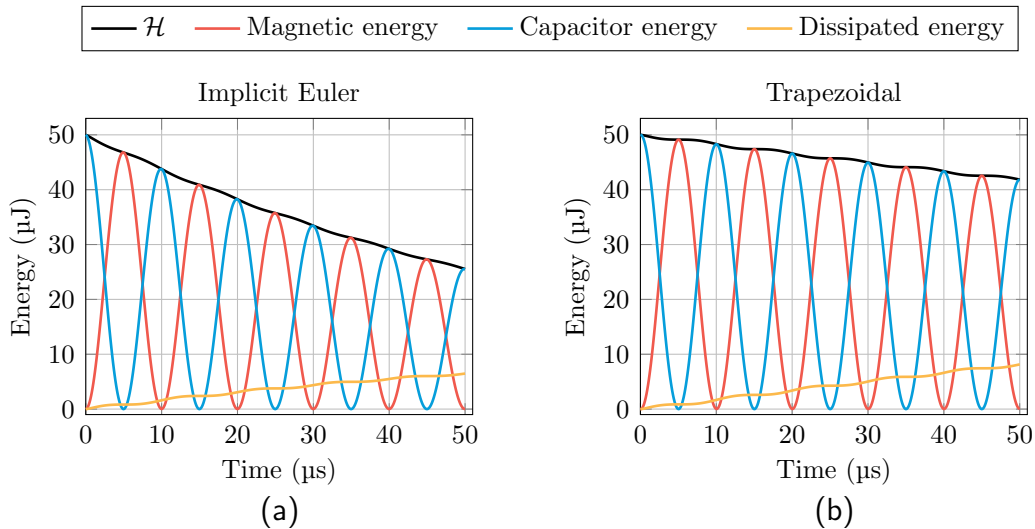


Figure 4: The energy of the oscillator with a conducting core when (a) the implicit Euler method and (b) the trapezoidal rule are used for time integration. The Hamiltonian contains again the contributions from the magnetic and the capacitor energies.

## Acknowledgments

This work was partially supported by the joint DFG/FWF Collaborative Research Centre CREATOR (DFG: Project-ID 492661287/TRR 361; FWF: 10.55776/F90) at TU Darmstadt, TU Graz and JKU Linz and by the Graduate School CE within Computational Engineering at the Technical University of Darmstadt.

## References

- [1] V. Mehrmann, B. Unger, Control of port-Hamiltonian differential-algebraic systems and applications, *Acta Numer.* 32 (2023) 395–515. doi:10.1017/S0962492922000083.
- [2] A. J. van der Schaft, D. Jeltsema, Port-Hamiltonian systems theory: an introductory overview, *Found. Trends Syst. Control* 1 (2–3) (2014) 173–378. doi:10.1561/26000000002.
- [3] S. Fiaz, D. Zonetti, R. Ortega, J. M. A. Scherpen, A. J. van der Schaft, A port-Hamiltonian approach to power network modeling and analysis,

- Eur. J. Control 19 (6) (2013) 477–485. doi:10.1016/j.ejcon.2013.09.002.
- [4] A. J. Malan, L. Rausche, F. Strehle, S. Hohmann, Port-Hamiltonian modelling for analysis and control of gas networks, IFAC-PapersOnLine 56 (2) (2023) 5431–5437. doi:10.1016/j.ifacol.2023.10.193.
- [5] A. J. van der Schaft, Port-Hamiltonian systems: Network modeling and control of nonlinear physical systems, in: H. Irschik, K. Schlacher (Eds.), *Advanced Dynamics and Control of Structures and Machines*, Springer Vienna, Austria, 2004, pp. 127–167. doi:10.1007/978-3-7091-2774-2\_9.
- [6] A. van der Schaft, Port-Hamiltonian modeling for control, *Annu. Rev. Control Robot. Auton. Syst.* 3 (2020) 393–416. doi:10.1146/annurev-control-081219-092250.
- [7] H. Hoang, F. Couenne, C. Jallut, Y. Le Gorrec, The port Hamiltonian approach to modeling and control of continuous stirred tank reactors, *Journal of Process Control* 21 (10) (2011) 1449–1458. doi:10.1016/j.jprocont.2011.06.014.
- [8] H. Ramirez, B. Maschke, D. Sbarbaro, Irreversible port-Hamiltonian systems: a general formulation of irreversible processes with application to the CSTR, *Chem. Eng. Sci.* 89 (2013) 223–234.
- [9] D. T. Tefera, S. Dubljevic, V. Prasad, A port Hamiltonian approach to dynamical chemical process systems network modeling and analysis, *Chem. Eng. Sci.* 261 (2022) 117907. doi:10.1016/j.ces.2022.117907.
- [10] O. Farle, D. Klis, M. T. Jochum, O. Floch, R. Dyczij-Edlinger, A port-Hamiltonian finite-element formulation for the Maxwell equations, in: *2013 International Conference on Electromagnetics in Advanced Applications (ICEAA)*, IEEE, 2013, pp. 324–327. doi:10.1109/iceaa.2013.6632246.
- [11] H. Gernandt, F. E. Haller, T. Reis, A. J. van der Schaft, Port-Hamiltonian formulation of nonlinear electrical circuits, *J. Geom. Phys.* 159 (2021) 103959. doi:10.1016/j.geomphys.2020.103959.

- [12] G. Haine, D. Matignon, F. Monteghetti, Structure-preserving discretization of Maxwell's equations as a port-Hamiltonian system, in: IFAC-PapersOnLine, Vol. 55, Elsevier, 2022, pp. 424–429. doi:10.1016/j.ifacol.2022.11.090.
- [13] A. Bartel, M. Clemens, M. Günther, B. Jacob, T. Reis, Port-Hamiltonian systems' modelling in electrical engineering, in: Scientific Computing in Electrical Engineering SCEE 2022, Mathematics in Industry, Springer, Berlin, 2021, pp. 133–143. doi:10.1007/978-3-031-54517-7\_15.
- [14] M. Clemens, M.-L. Henkel, F. Kasolis, M. Günther, A port-Hamiltonian system perspective on electromagneto-quasistatic field formulations of Darwin-type, Preprint arxiv:2404.18767, Cornell University (2024). doi:10.48550/arXiv.2404.18767.
- [15] A. Macchelli, C. Melchiorri, Modeling and control of the Timoshenko beam. The distributed port Hamiltonian approach, SIAM J. Control Optim. 43 (2) (2004) 743–767. doi:10.1137/S0363012903429530.
- [16] R. Altmann, P. Schulze, A port-Hamiltonian formulation of the Navier–Stokes equations for reactive flows, Systems Control Lett. 100 (2017) 51–55. doi:10.1016/j.sysconle.2016.12.005.
- [17] R. Rashad, S. Stramigioli, The port-Hamiltonian structure of continuum mechanics, J. Nonlinear Sci. 35 (35) (2025). doi:10.1007/s00332-025-10130-1.
- [18] A. Warsewa, M. Böhm, O. Sawodny, C. Tarín, A port-Hamiltonian approach to modeling the structural dynamics of complex systems, Appl. Math. Model. 89 (2021) 1528–1546. doi:10.1016/j.apm.2020.07.038.
- [19] T. Breiten, R. Morandin, P. Schulze, Error bounds for port-Hamiltonian model and controller reduction based on system balancing, Comput. Math. with Appl. 116 (2022) 100–115. doi:10.1016/j.camwa.2021.07.022.
- [20] A. Brugnoli, R. Rashad, S. Stramigioli, Dual field structure-preserving discretization of port-Hamiltonian systems using finite element exterior calculus, J. Comput. Phys. 471 (2022) 111601. doi:10.1016/j.jcp.2022.111601.

- [21] J. Giesselmann, A. Karsai, T. Tscherpel, Energy-consistent Petrov–Galerkin time discretization of port-Hamiltonian systems, Preprint arxiv:2404.12480, Cornell University (2024). doi:10.48550/arXiv.2404.12480.
- [22] S. Gugercin, R. V. Polyuga, C. Beattie, A. van der Schaft, Structure-preserving tangential interpolation for model reduction of port-Hamiltonian systems, *Automatica* 48 (9) (2012) 1963–1974. doi:10.1016/j.automatica.2012.05.052.
- [23] P. Kotyczka, L. Lefèvre, Discrete-time port-Hamiltonian systems: a definition based on symplectic integration, *Systems Control Lett.* 133 (2019) 104530. doi:10.1016/j.sysconle.2019.104530.
- [24] M. Seslija, J. M. A. Scherpen, A. J. van der Schaft, Explicit simplicial discretization of distributed-parameter port-Hamiltonian systems, *Automatica* 50 (2) (2014) 369–377.
- [25] R. Altmann, P. Schulze, A novel energy-based modeling framework, *Math. Control Signals Systems* (2025). doi:10.1007/s00498-024-00405-5.
- [26] C. Beattie, V. Mehrmann, H. Xu, H. Zwart, Linear port-Hamiltonian descriptor systems, *Math. Control Signals Systems* 30 (2018) 17. doi:10.1007/s00498-018-0223-3.
- [27] V. Mehrmann, R. Morandin, Structure-preserving discretization for port-Hamiltonian descriptor systems, in: *Proceedings of the 58th IEEE Conference on Decision and Control, Nice, France, 2019*, pp. 6863–6868. doi:10.1109/CDC40024.2019.9030180.
- [28] C. Mehl, V. Mehrmann, M. Wojtylak, Linear algebra properties of dissipative Hamiltonian descriptor systems, *SIAM J. Matrix Anal. Appl.* 39 (3) (2018) 1489–1519. doi:10.1137/18M1164275.
- [29] A. Arkkio, Analysis of induction motors based on the numerical solution of the magnetic field and circuit equations, Phd thesis, Helsinki University of Technology, urn:nbn:fi:tkk-001267 (12 1987).

- [30] L. Bortot, B. Auchmann, I. Cortes Garcia, A. M. Fernando Navarro, M. Maciejewski, M. Mentink, M. Prioli, E. Ravaioli, S. Schöps, A. Verweij, STEAM: A hierarchical co-simulation framework for superconducting accelerator magnet circuits, *IEEE Trans. Appl. Super.* 28 (3), arxiv:1801.08957 (04 2018). doi:10.1109/TASC.2017.2787665.
- [31] G. Bedrosian, A new method for coupling finite element field solutions with external circuits and kinematics, *IEEE Trans. Magn.* 29 (2) (1993) 1664–1668. doi:10.1109/20.250726.
- [32] H. De Gersem, K. Hameyer, A finite element model for foil winding simulation, *IEEE Trans. Magn.* 37 (5) (2001) 3427–3432. doi:10.1109/20.952629.
- [33] S. Schöps, H. De Gersem, T. Weiland, Winding functions in transient magnetoquasistatic field-circuit coupled simulations, *COMPEL* 32 (6) (2013) 2063–2083. doi:10.1108/COMPEL-01-2013-0004.
- [34] E. Paakkunainen, J. Bundschuh, I. C. Garcia, H. De Gersem, S. Schöps, A stabilized circuit-consistent foil conductor model, *IEEE Access* 12 (2024) 1408–1417, arxiv:2306.13477. doi:10.1109/ACCESS.2023.3346677.
- [35] D. Estévez Schwarz, C. Tischendorf, Structural analysis of electric circuits and consequences for MNA, *Int. J. Circ. Theor. Appl.* 28 (2) (2000) 131–162. doi:10.1002/(SICI)1097-007X(200003/04)28:2<131::AID-CTA100>3.0.CO;2-W.
- [36] A. Bartel, S. Baumanns, S. Schöps, Structural analysis of electrical circuits including magnetoquasistatic devices, *APNUM* 61 (2011) 1257–1270. doi:10.1016/j.apnum.2011.08.004.
- [37] I. Cortes Garcia, S. Schöps, H. De Gersem, S. Baumanns, Systems of differential algebraic equations in computational electromagnetics, in: *Applications of Differential-Algebraic Equations: Examples and Benchmarks*, *Differential-Algebraic Equations Forum*, Springer, Heidelberg, 2019. doi:10.1007/11221\_2018\_8.
- [38] J. D. Jackson, *Classical Electrodynamics*, 3rd Edition, Wiley & Sons, New York, NY, USA, 1998. doi:10.1017/CB09780511760396.

- [39] C. R. I. Emson, C. W. Trowbridge, Transient 3d eddy currents using modified magnetic vector potentials and magnetic scalar potentials, *IEEE Trans. Magn.* 24 (1) (1988) 86–89. doi:10.1109/20.43862.
- [40] R. Albanese, G. Rubinacci, Integral formulation for 3D eddy-current computation using edge elements, *IEE Proc. Sci. Meas. Tech.* 135 (7) (1988) 457–462. doi:10.1049/ip-a-1:19880072.
- [41] P. Monk, *Finite Element Methods for Maxwell's Equations*, Oxford University Press, Oxford, 2003.
- [42] A. Nicolet, F. Delincé, Implicit Runge-Kutta methods for transient magnetic field computation, *IEEE Trans. Magn.* 32 (3) (1996) 1405–1408. doi:10.1109/20.497510.
- [43] I. Cortes Garcia, *Mathematical analysis and simulation of field models in accelerator circuits*, Dissertation, Technische Universität Darmstadt, Darmstadt, Springer Theses: Recognizing Outstanding Ph.D. Research (2020). doi:10.1007/978-3-030-63273-1.
- [44] P. Dular, C. Geuzaine, Spatially dependent global quantities associated with 2-d and 3-d magnetic vector potential formulations for foil winding modeling, *IEEE Trans. Magn.* 38 (2) (2002) 633–636. doi:10.1109/20.996165.
- [45] F. Zhang, *The Schur Complement and Its Applications*, Springer, New York, NY, USA, 2005. doi:10.1007/b105056.
- [46] C.-W. Ho, A. E. Ruehli, P. A. Brennan, The modified nodal approach to network analysis, *IEEE Trans. Circ. Syst.* 22 (6) (1975) 504–509. doi:10.1109/TCS.1975.1084079.
- [47] P. Dular, C. Geuzaine, F. Henrotte, W. Legros, A general environment for the treatment of discrete problems and its application to the finite element method, *IEEE Trans. Magn.* 34 (5) (1998) 3395–3398. doi:10.1109/20.717799.
- [48] C. Geuzaine, J.-F. Remacle, Gmsh: A 3-D finite element mesh generator with built-in pre- and post-processing facilities, *Int. J. Numer. Meth. Eng.* 79 (2009) 1309–1331. doi:10.1002/nme.2579.